THE JOURNAL OF PHYSICAL CHEMISTRY B

Article

pubs.acs.org/JPCB

Observation on the Ion Association Equilibria in $NaNO_3$ Droplets Using Micro-Raman Spectroscopy

Jun-Ying Yu,[†] Yun Zhang,[†] See-Hua Tan,[†] Yong Liu,*[,‡] and Yun-Hong Zhang*[,†]

[†]The Institute of Chemical Physics, Key Laboratory of Cluster Science, School of Chemistry, Beijing Institute of Technology, Beijing 100081, People's Republic of China

[‡]Department of Chemistry, University of Colorado—Denver, Denver, Colorado 80217, United States

Supporting Information

ABSTRACT: Ion association ratios as a function of concentration were estimated in single $NaNO_3$ droplets (5−60 μm) on a polytetrafluoroethylene (PTFE) substrate with molar water-to-solute ratios (WSRs) of 0.8−28 and bulk $NaNO_3$ solutions with WSRs of 35−200 by combining micro-Raman spectroscopy and component band analysis. Concentrations of the $NaNO_3$ droplets were accurately controlled by adjusting relative humidity (RH) in a sample chamber. As the WSRs decreased from 200 to 0.8, symmetric stretching band (ν_1-NO_3^-) was observed to shift from 1047 to 1058 cm^{-1} along with a change in full width at half-maximum (fwhm) from ∼10 to ∼16 cm^{-1}, indicative of formation of ion pairs with different structures. Through the component band analysis of the ν_1-NO_3^- band, five bands centered at 1040.0, 1042.9, 1048.5, 1053.5, and 1057.0 cm^{-1} were identified and assigned to coupled wagging modes of water molecules hydrated with nitrate ions, free hydrated nitrate anions, solvent-shared ion pairs (SIPs), contact ion pairs (CIPs), and the complex ion aggregates (CIAs), respectively. There were large amounts of SIPs and CIPs in dilute $NaNO_3$ solution even at an extremely low concentration (WSR ∼ 200), and each accounted for 50% and 20% of total nitrate species, respectively. This finding is in good agreement with earlier reported observations. In the dilute solutions (45 < WSR < 200), there is the same amount of free hydrated ions transformed into SIPs as that of SIPs transformed into CIPs. As a result, the overall amount of SIPs remained unchanged over the concentration range. With a decrease in WSR from 45 to 0.8, the amounts of SIPs and free solvated NO_3^- ions kept decreasing, whereas the amount of CIPs rose to a maximum at WSR = 7 and then fell with a further decreasing WSR. Formation of CIAs started at WSR ∼ 45, and its amount continuously increased as the WSR is further reduced to 0.8. The effect of temperature on ion association structure in the $NaNO_3$ droplets was also studied in the present work. An increase in temperature promoted formation of both CIPs and CIAs, and the latter was more pronounced. At 80 °C, the most concentrated $NaNO_3$ droplets had a WSR approximately equal to 0.12 and were in amorphous state with cations and anions aggregated in a complicated manner, highly similar to ionic liquid.

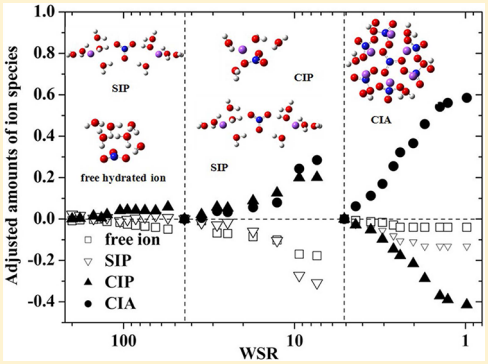

INTRODUCTION

Ion pairing occurs universally in electrolyte solutions and has been known important in chemical reactions, surface reactivity, solvent selection, crystal formation, and biological metabolism.[1−6] In electrolyte solutions, oppositely charged ions associate with each other by long-range electrostatic forces and can exist in one of four forms, namely (1) free solvated ions with intact first solvation shells, (2) solvent-separated ion pairs with a single solvent layer between cation and anion, (3) contact ion pair with both cation and anion contacting directly, and (4) complex ion aggregates with association of contact ion pairs.[4,6]

Since ion association was revealed in solutions, many theories have been developed to explain the ion pairing.[6−11] Arrhenius first proposed electrolytic dissociation theory dating back to early 1880s and assumed an electrolyte such as NaCl partially dissociated in water in a form of active ion. He also estimated degrees of association for various electrolytes in water using electrical conductivity and freezing point data.[7] Thereafter, Debye−Hückel postulated dilute solution would undergo complete dissociation of electrolytes.[9] Bjerrum later introduced a concept of ion pairing of strong electrolytes based on Brönsted's theory of specific ionic interactions and stated that ion pairs would be unlikely to be present in a solution made of AB type of electrolyte such as NaCl.[10,11] In addition to the theoretical studies, ion pairing has also been experimentally investigated through measurements of conductivity,[7,12−14] activity,[14,15] and relaxation.[16,17] A remarkable development in understanding relationship between various types of ion pairs was the establishment of Eigen mechanism by Eigen and Tamm through the ultrasonic relaxation technique.[18,19] According to the Eigen mechanism, the equilibrium equations from free

Received: June 28, 2012
Revised: August 23, 2012
Published: September 24, 2012

dx.doi.org/10.1021/jp306367v | J. Phys. Chem. B 2012, 116, 12581−12589

aqueous ions to contact ion pairings in solutions can be represented as follows:

$$M^{m+}(aq) + L^{n-}(aq) \underset{\text{free}}{} \leftrightarrow [M^{m+}(OH_2)(OH_2)L^{n-}](aq) \underset{\text{2SIP}}{} \leftrightarrow [M^{m+}(OH_2)L^{n-}](aq) \underset{\text{SIP}}{} \leftrightarrow [ML]^{(m-n)+}(aq) \underset{\text{CIP}}{}$$

in which free hydrated ions combine to form double solvent-separated ion pairs (2SIP), followed by further water loss to form solvent-shared ion pairs (SIPs) and contact ion pairs (CIPs). This mechanism has been used to explain ion association in supersaturated $NaClO_4$ droplets[20] and $MgSO_4$ solutions.[21] Nevertheless, recently Zhang et al. also found that not all ion association processes in electrolyte solutions follow the Eigen mechanism.[22−24] Furthermore, spectroscopic methods, including Raman spectroscopy, have also been widely used in the studies of complex formation and ion association. Raman spectroscopy can offer spectral features of each species formed in solution with high signal-to-noise ratio (S/N);[25−32] however, spectra often do not have enough resolution to distinguish individual peaks and instead only provide overlapped vibration bands of a complex mixture. For this reason, it is necessary to use additional tools such as component band analysis to separate spectra and evaluate their relative ratios.[32−36]

Over years, nitrate solutions such as $NaNO_3$ have emerged as a model system for ion association study, and a great deal of effort has been directed to it. Mathieu and Lounsbury[29] discovered cations and solvent can affect NO_3^- ions in metallic nitrate solutions using Raman spectroscopy. By analyzing Raman and infrared spectra of alkali metal nitrate solutions, Irish and Davis[33,34] found that contact ion pairs between nitrate and alkali metallic ions were formed by increasing the concentration. With Raman spectroscopy, Xu et al. concluded that larger size and lower charge density of a cation would facilitate formation of contact ion pairs in metal nitrate aqueous solutions.[25] Vollmar[27] looked into KNO_3 and $NaNO_3$ solutions and noticed that even though the less hydrated K^+ was more favorable for ion pairing than Na^+, Na^+ actually formed ion pairs with NO_3^- more easily than K^+ in their individual aqueous solutions because of hydration effect overcome by a lager intrinsic "crystal" effect or Na^+ polarizing power. The author also found that Na^+ easily formed ion pairs with NO_3^- even with concentrations less than 3 mol/L. Caminiti et al. relied on X-ray diffraction to confirm presence of $M^+WNO_3^-$ type ionic interactions in two concentrated aqueous solutions (5 and 7 M) of $NaNO_3$. They also calculated coordination numbers of the hydrated Na^+ and NO_3^- to be 6 and 3−6, respectively.[37] Riddell et al. revealed presence of both $Na^+NO_3^-$ ion pairs and solvated nitrate ions in $NaNO_3/D_2O$ solutions by Raman and infrared spectroscopy and obtained thermodynamic association constant by an extrapolation procedure.[38] On the basis of band-component analysis, Frost and James found differences of association equilibria for mixed $NaNO_3$/NaCl aqueous solutions, mixed $NaNO_3/H_2O/D_2O$ solutions, and pure $NaNO_3$ aqueous solutions. They also observed that formation of both solvent-shared ion pairs and contact ion pairs was favored by lower temperatures.[39] In spite of many studies, at present our knowledge of the association equilibrium in $NaNO_3$ aqueous solutions over a wide range of concentration (from extremely dilute to supersaturated solutions) remains scarce.

One reason that nitrate salt aqueous solutions have received significant interests is due to its special symmetry structure[29,34,40−42] An isolated NO_3^- ion is planar and has a D_{3h} symmetry with all three equivalent N−O bonds and bond angles of 120°. In nitrate salt solution, such symmetry can be broken by water molecules[40,43−45] and cations[25,27−30] and be reduced to C_{2v} or C_s symmetries. Also, nitrate salts have great abundance in atmosphere and can potentially impact climate system and atmospheric environment.[46−48] For example, sodium nitrate, mainly produced from heterogeneous reaction between sea salt particles and atmospheric nitrogen oxides such as NO_2, NO_3, N_2O_5, and HNO_3,[48−53] is a major component of marine aerosols. Recently, it has received much attention, especially about its hygroscopic properties.[54−63] Despite extensive studies, there are still discrepancies in its deliquescence and efflorescence process. Tang and co-workers[60,64] used the single-particle levitation technique to study hygroscopic properties of $NaNO_3$ and reported their deliquescence relative humidity (DRH) and efflorescence relative humidity (ERH) at ∼75% and ∼35%, respectively. Recently, Ghorai and Tivanski employed scanning transmission X-ray microscopy and NEXAFS to investigate an individual deposited $NaNO_3$ particle and observed similar results.[65] In contrast, many groups showed $NaNO_3$ particles do not have distinct DRH and ERH and only present continuous growth and shrinkage during hydration and dehydration processes using different types of analytical techniques such as micro-FT-IR spectroscopy,[56] attenuated total reflection FT-IR,[66] a hygroscopicity tandem differential mobility analyzer (H-TDMA),[64,67] an analyzer with a thermal conductivity detector,[63] environmental scanning electron microscopy (ESEM),[54] and a multianalysis aerosol reactor system (MAARS).[68] Such different behaviors of the $NaNO_3$ systems likely arise from different nucleation mechanisms. As a result, it is needed to carry out further studies in interactions between ions and between water molecules and ions in $NaNO_3$ droplets to provide more insights into its hygroscopic behaviors.

Temperature in the troposphere spans over a wide range. Recent studies have indicated that ambient temperature affects phase, scattering efficiency and optical properties of aerosol particles, and interactions between ions in solution.[69,70] At present, our knowledge regarding how temperature affects ion structure at molecular level is still limited and sometimes contradictory. For instance, Spohn and Brill found that at high pressure ions tended to transform from solvent-separated ion pairs to contact ion pairs with increasing temperatures in aqueous $NaNO_3$ solutions.[71] In contrast, Frost and James observed both solvent-separated ion pairs and contact ion pairs were disfavored in the $NaNO_3$ solutions, and the free hydrated ions were favored as the temperature increased within the range of −5 to 65 °C.[39]

Investigations of ion pairing in bulk solutions of electrolyte were often limited by solubility of solute in a solvent.[38,39] In this work single $NaNO_3$ droplets deposited on a hydrophobic substrate were used as they can easily achieve a supersaturated state with enhanced ion interactions by simply decreasing ambient relative humidity (RH). The deposited droplets had spheric shape with slight irregularity due to gravity, and this helped avoid strong disturbance of the MDRs (morphology-dependent resonances) on Raman spectra. Diameters of the

droplets ranged from 5 to 60 μm, relevant to atmospheric aerosol particles. *In situ* Raman spectra of single $NaNO_3$ droplets with high S/N were acquired at various RHs ranging from 94 to 27% (i.e., WSRs from 28 to 0.8) with a micro-Raman technique. In addition, a series of Raman measurements of bulk $NaNO_3$ solutions with WSRs of 35−200 were carried out to complement the data in low concentration. Raman spectra were analyzed using component band analysis to obtain relative ratios of four ionic species: free hydrated nitrate anions, solvent-shared ion pairs, contact ion pairs, and complex ion aggregates as a function of the concentration of $NaNO_3$ droplets as well as its bulk solutions. According to the evolution in the Raman line shape and the position of the NO_3^- (ν_1 NO_3^-) symmetric stretching band as a function of concentration, ion association equilibria between the free hydrated NO_3^- ions, the solvent-shared ion pairs (SIPs), the contact ion pairs (CIPs), and the complex ion aggregates (CIAs) were investigated. In addition, we also reported effect of ambient temperature on ion association in the $NaNO_3$ solution.

EXPERIMENTAL SECTION

Sample Preparation. Bulk $NaNO_3$ aqueous solutions with different WSRs (35−200) were prepared by dissolving analytical grade $NaNO_3$ into triply distilled water (Barnstead EASY pure II) without further purification. Using a syringe, $NaNO_3$ droplets (5−60 μm in diameter) were dispensed onto a hydrophobic substrate with a piece of quartz slide covered by a hydrophobic PTFE (polytetrafluoroethylene) film. The substrate was then mounted to the bottom of a chamber which was sealed with a thin transparent PE (polyethylene) film. To increase S/N ratio, we first selected larger droplets for Raman spectra acquisition under higher RHs condition. After transformation of larger droplets into crystal with a decreasing ambient RH, smaller droplets were selected to obtain spectra at low RHs. RHs in the chamber were adjusted by mixing a stream of dry N_2 with another stream of water-saturated N_2 at controlled flow rates. The RH and temperature were recorded by a hygrometer (Centertek Center310) with an accuracy of ±2.5% and ±0.7 °C.

Apparatus and Conditions for the Measurements. Figure 1 shows the schematic diagram of experiment setup used in this work, including (a) micro-Raman spectrometer and (b) physisorption analyzer. The micro-Raman system (Renishaw Invia), equipped with a Leica DMLM microscope for observing morphological changes of the droplets and focalizing the laser on the droplets, was used to obtain the Raman spectra. A 514.5 nm Ar^+ laser (LS-514 model, Laser Physics) with an output power of 20 mW was used as the excitation source. With a pinhole in place, the laser beam was focused on the sample with a diameter of ~1 μm. A 514.5 nm Raman notch filter was used to remove the strong Rayleigh scatting. Before the Raman measurement, spectra were calibrated using 520 cm^{-1} silicon band as standard. After passing through a 1800 grooves/mm grating, backscattering signal was detected by a charge-coupled device (CCD). Raman spectra in the range of 200−4000 cm^{-1} were averaged over three scans, and each one had a scanning time of 10 s. To ensure droplets in the chamber completely equilibrate with ambient RH, it took about 40 min for droplets to stabilize at any given RHs before each Raman measurement. Most spectra were collected at room temperature with a small variation from 22 to 24 °C. Experiments at higher temperatures were achieved by a temperature controlling unit on the micro-Raman spectrometer. All of the spectra were acquired by Wire 2.0 program supplied by Renishaw.

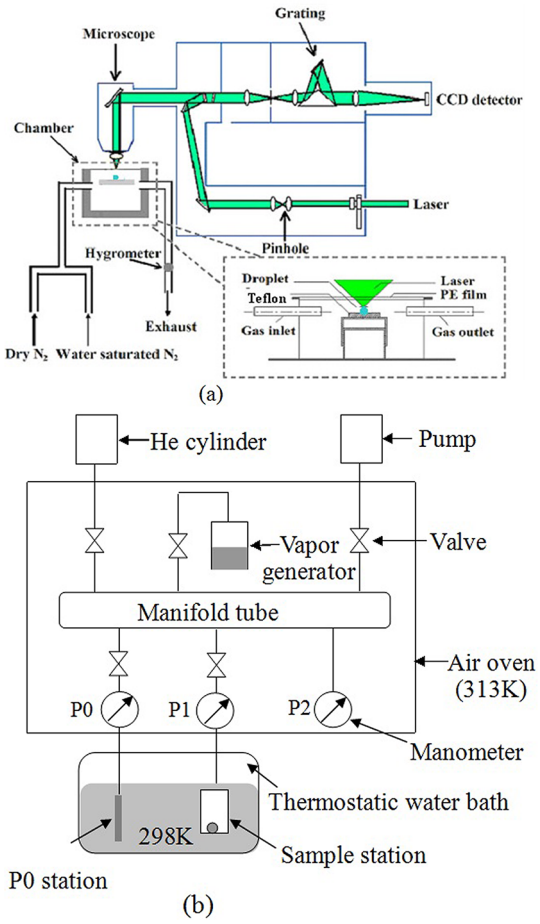

Figure 1. Schematic diagram of the experiment setup: (a) micro-Raman spectrometer and (b) physisorption analyzer.

The isothermal adsorption of $NaNO_3$ was obtained by a physisorption analyzer, which was composed of a Belsorp-max with Belprep II (BEL JAPAN, INC.) and a low-temperature thermostat (Beijing Bilang). Its schematic diagram is shown in Figure 1b. A stainless steel manifold tube (V = 18.6632 cm^3), which was connected to a turbo pump, a helium port, a vapor generator, a P0 station, and a sample station, was kept in a constant temperature (298 ± 0.5 K) chamber to avoid vapor condensation during vapor adsorption experiments. Before adsorption, the sample tube was purged with helium. During the adsorption process, pressure change resulting from gas loss was monitored by three manometers for the manifold tube, the P0 station, and the sample station. The same process was repeated until pressure change was less than 0.3% within 30 min, which was considered to be equilibrated.

Spectra Fitting. In order to investigate the interactions among Na^+, NO_3^-, and H_2O in $NaNO_3$ solutions, band component analysis was implemented to analyze evolution of symmetric stretching vibration of NO_3^- ions for all spectra obtained in the range of 1020−1080 cm^{-1} using a Gaussian function built in Origin 7.0 for nonlinear curve fitting. The function is expressed as follows:

$$y = y_0 + \frac{A}{\omega\sqrt{\pi/2}} e^{-2(x-x_c)^2/\omega^2}$$

dx.doi.org/10.1021/jp306367v | J. Phys. Chem. B 2012, 116, 12581−12589

where y_0 is the baseline offset, A is the integral area, x_c is the center of the peak, and ω is the full width of the peak at half-maximum (fwhm). y_0 was normally kept as zero, and values of x_c and ω were obtained in the following steps. The frequency and the fwhm of each component band at any RHs were first acquired individually based on best matches between fitted curves and experimental data. An allowable range of each parameter was kept constant for curve fitting of all spectra over the whole RH range. Average values of the frequencies and the fwhms were then calculated and used to fit the spectra again with a smaller range of parameters. Such process was repeated until the frequency and the fwhm of each band converged and became constant. At last, all parameters were kept constant for each components (i.e., free solvated NO_3^- ions, solvent-shared ion pairs, contact ion pairs, and complex ion aggregates) throughout the fitting process except for the integrals, A, of each component, which were the only fitting parameters to achieve best final spectral fitting.

RESULTS AND DISCUSSION

Supersaturated $NaNO_3$ Droplets on a Hydrophobic Substrate. The molar water-to-solute ratios (WSRs) of $NaNO_3$ droplets at various RHs are displayed in Figure 2.

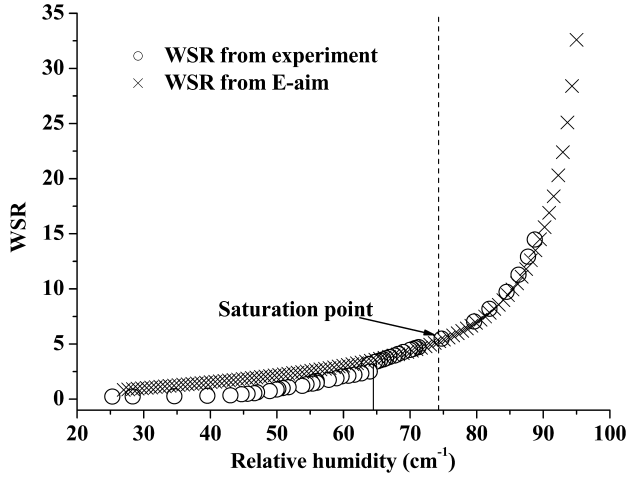

Figure 2. Molar water-to-solute ratios (WSRs) of $NaNO_3$ droplets at various RHs: hollow circles, WSRs obtained by the physisorption analyzer in this work; crosses, WSRs obtained by using the extended aerosol inorganic model (E-AIM).

Data points (hollow circles) obtained by the physisorption analyzer in experiments are consistent with those predicted by the extended aerosol inorganic model (E-AIM).[72−74] As ambient RH decreased, the droplets deposited on the hydrophobic substrate gradually lost water and became more concentrated. They did not undergo sudden crystallization at the saturation point (RH = 74.5%, WSR = 5.2);[59,60] instead, they became supersaturated with a further decrease in RH. Such hysteresis is commonly observed for atmospheric aerosols with deliquescent and effluorescent behaviors. As the RH dropped to 64%, with continuous water loss, some droplets started to crystallize, resulting in an inflection point on the RH-WSR curve in Figure 2. When the RH further decreased down to ~27% (WSR = 0.8), many droplets were still in supersaturated state and have not undergone efflorescence, and each Na^+ and NO_3^- ion in those supersaturated droplets only shared less than one water molecule. Such a supersaturated state was favorable for the formation of ion pairs between Na^+ and NO_3^-, which can be detected *in situ* by micro-Raman spectroscopy.

Raman Spectra of $NaNO_3$ Aqueous Solutions with Different WSRs. Figure 3 shows vibration bands of NO_3^- for

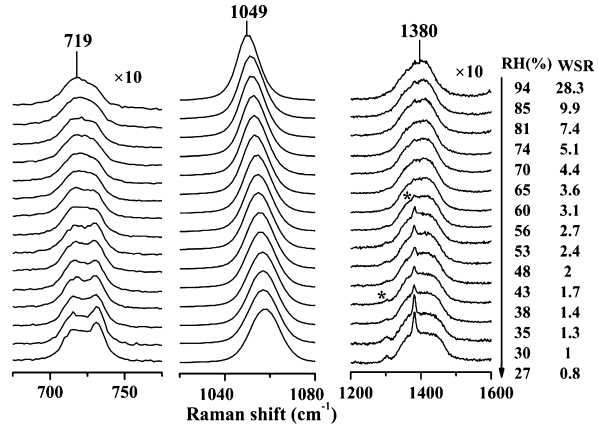

Figure 3. Raman spectra of $NaNO_3$ droplets at various RH values during the efflorescence process.

$NaNO_3$ droplets with WSRs in the range of 0.8−28 (94−27% RH). All spectra are normalized to the intensity of the ν_1-NO_3^- band. Raman spectra of $NaNO_3$ in dilute bulk solutions (WSR > 45) are not shown here. Lager droplets with a diameter of ~60 μm were selected to obtain the spectra at higher RHs for their higher S/N ratios. As the ambient RH decreased under the saturation point at RH = 74.5%, larger droplets were found to be more readily to crystallize. Because the hysteresis phenomenon is more prominent for smaller droplets, we were able to acquire Raman spectra of highly concentrated $NaNO_3$ droplets at lower RHs by searching for the smaller ones. The smallest droplets with a diameter of ~5 μm used in the study did not crystallize even at RHs lower than 27% (WSR = 0.8). Note the quality of the Raman spectra was fairly good even for smaller droplets which enabled to provide reliable structural information on $NaNO_3$ solutions in the supersaturated state.

The planar free NO_3^- ion with a D_{3h} symmetry has four fundamental vibration bands: in-phase symmetric stretching band ν_1 (A_1') at ~1049 cm^{-1}, out-of-plane deformation band ν_2 (A_2'') at ~830 cm^{-1}, out-of-phase stretching band ν_3 (E') at ~1380 cm^{-1}, and in-plane bending band ν_4 (E') at ~719 cm^{-1}. The ν_3 and ν_4 are active in both infrared and Raman, while the ν_1 is only Raman-active and the ν_2 is only infrared-active.[25,28,30,33,34,75] Figure 3 exhibits Raman spectra of $NaNO_3$ aqueous solutions at various RH values during an efflorescence process. As the ambient RHs decreased, the ν_1-NO_3^- bands experienced continuous blue-shifts. Meanwhile, a new distinct band appeared at ~730 cm^{-1} as a shoulder of ν_4-NO_3^- band (~719 cm^{-1}) accompanying the formation of contact ion pairs. This is consistent with literature findings.[25,28,29] Strong interactions between Na^+ and NO_3^- ions also broadened the ν_3-NO_3^- band with increasing concentrations.[25,35,47]

The ν_1-NO_3^- band has been known to be sensitive to cation type, salt concentration, and temperature.[1,39,76] Figure 4 shows peak position and fwhm of the ν_1-NO_3^- band for $NaNO_3$ solutions as a function of WSR. Results from droplets with WSRs of 0.8−28 and bulk solutions with WSRs of 35−200 are also included. In the dilute solutions (WSR > 45), both the

dx.doi.org/10.1021/jp306367v | J. Phys. Chem. B 2012, 116, 12581−12589

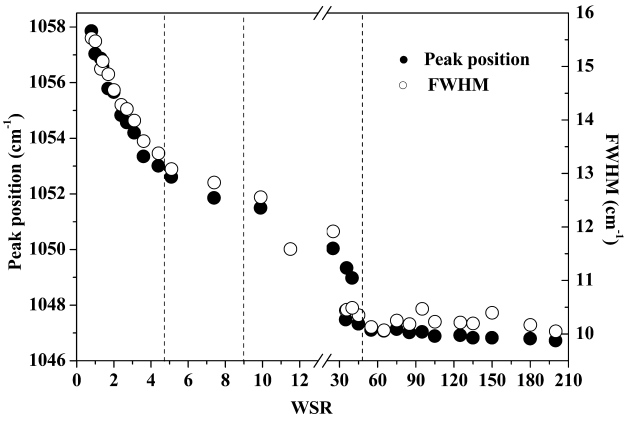

Figure 4. Peak position and the fwhm of the ν_1-NO_3^- band of $NaNO_3$ solutions with WSR in the range of 200−0.8.

peak position and the fwhm of the ν_1-NO_3^- band were seemingly independent of changes in concentration and remained nearly constant. As the WSR decreased from 45 to 9, both the frequency and the fwhm increase rapidly from 1047 to 1051.5 cm^{-1} and from 10.4 to 12.5 cm^{-1}, respectively. As the WSR decreased further from 9 to 5, the increases slowed down slightly. Then in the supersaturated region with WSR less than 5.1, the frequency and the fwhm picked up the pace again and finally reached ∼1057.8 and ∼15.5 cm^{-1} at WSR = 0.8. The characteristic evolution of ν_1-NO_3^- band resulted from the formation of Na^+−NO_3^- ion pairs with different special structures.[25,27,39,55] Detailed analyses are to be presented in the followed sections.

Component Analysis of the ν_1-NO_3^- Band. NO_3^- ions with different structures would present different Raman spectral features. The Raman spectrum of $NaNO_3$ solution in the range of 1020−1080 cm^{-1} is not only originated from NO_3^- but various ion pairs species as well, including free hydrated ion, solvent-shared ion pair and contact ion pair, and complex ion aggregate depending on concentration.[24,26,38,39,55]

Na^+ was found to form ion pairs very easily with NO_3^- even when the concentration was below 3 mol dm^{-3} (WSR ∼ 15.6).[27] As illustrated in the Figure 4, the formation of ion pairs altered peak position and fwhm of ν_1-NO_3^-. To understand the interactions between Na^+ and NO_3^- as a function of concentration in aqueous solution, a curve fitting process as described in the Experimental Section was applied to separate individual component bands and determine their contribution to the band envelope of ν_1-NO_3^-.

Raman spectra in the range of 1020−1080 cm^{-1} at various WSRs and their corresponding fitted bands are shown in Figure 5. Besides the three bands centered at 1043, 1048.5, and 1053.5 cm^{-1}, which are assigned to free hydrated nitrate anions, solvent-shared ion pairs (SIP), and contact ion pairs (CIP), respectively, two additional component bands (complex ion aggregates and coupling vibration of water near NO_3^-) were introduced to better fit the spectra. The optimized geometries of several ion species are shown in the Supporting Information (Figure). The peak position, fwhm, and assignments of five fitted bands derived from the contour of ν_1-NO_3^- band are given in Table 1. With a decrease in WSR, the contact ion pairs would lose water further and transform into complex ion aggregates (CIAs), resulting in a blue-shift in peak position of ν_1-NO_3^- band to 1058 cm^{-1}. In addition, another band located at a lower frequency of ∼1040.0 cm^{-1} was weakened with

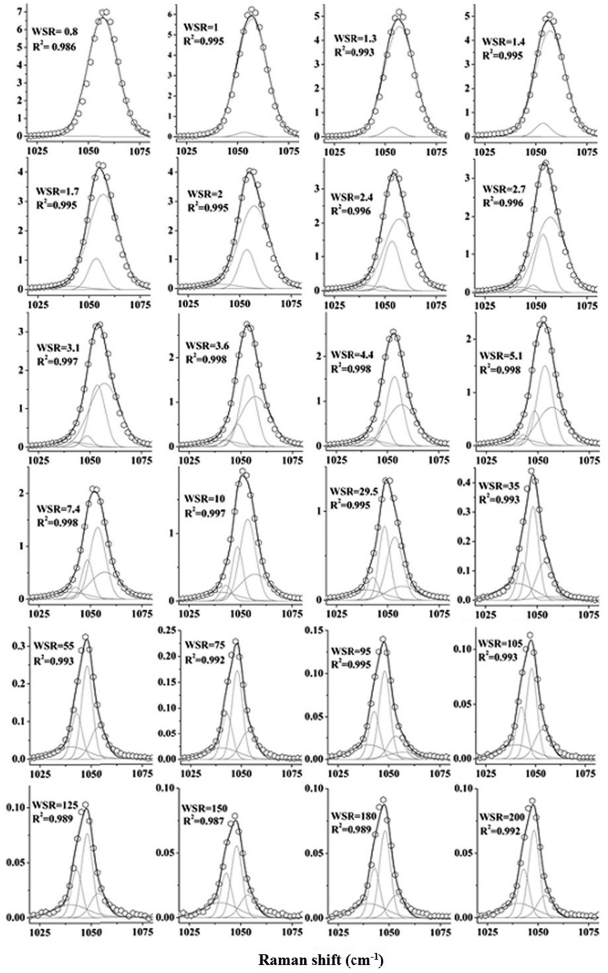

Figure 5. Experimental and fitted spectra in the region of 1020−1080 cm^{-1}: hollow hexagons, the experimental Raman spectra; gray solid lines, the five fitted spectral components; black solid lines, the sum spectra of the five fitted spectral components; R^2, the coefficient of determination.

Table 1. Assignments for Resolved Components of the ν_1-NO_3^-

assignments	peak position (cm^{-1})	fwhm (cm^{-1})
coupling vibrations of water near the NO_3^-	1040	20
solvated nitrate anion	1042.9	5.76
solvent-shared ion pair	1048.5	5.9
contact ion pair	1053.5	8.83
complex ion aggregates	1057	17.2

increasing NO_3^- concentrations. It was assigned to coupling vibration of inner shell water adjacent to the NO_3^- ions. This will be discussed in more detail in the following section. In our work, the SIPs and CIPs were found in very dilute solutions (WSR ∼ 200), which would not be impossible according to the Debye−Hückel theory. Moreover, a band at ∼1057 cm^{-1} assigned to the CIAs began to show up at WSR ∼45, and this has never been observed before.[24,55] The NO_3^- symmetric stretching of the solid $NaNO_3$ we measured located at about 1067 cm^{-1}, far from the ion pair components, and did not appear in the spectra of $NaNO_3$ droplets during dehumidifying process from 94% to 27%. Therefore, No $NaNO_3$ crystals were

dx.doi.org/10.1021/jp306367v | J. Phys. Chem. B 2012, 116, 12581−12589

formed in the droplets with RH > 27%, and no contribution of solid $NaNO_3$ was taken into account in the component analysis.

Figure 6 exhibits distribution of different ion species and degree of ion association as a function of WSR. A relative amount of different ion species was obtained from area ratio of each fitted band to sum of the four fitted bands. In the dilute solutions with WSRs ranging from 200 to 45, three different ion species (free hydrated ions, SIPs, and CIPs) coexisted, and the SIPs were the most dominant one. Within this WSR range, the amount of SIPs remained almost unchanged with increasing $NaNO_3$ concentrations, whereas the amounts of free hydrated NO_3^- ions and CIPs slightly decreased and increased, respectively. As the WSRs further decreased below 45, the amount of free hydrated ions decreased more rapidly and that of SIPs began to decrease. The formation of CIAs started at WSR ~ 45 and their amount increased with increasing concentrations. The amount of CIPs increased rapidly as the WSRs dropped from 45 to 9 and then decreased as the WSRs dropped further from 5 to 0.8. When RH was lowered below the saturation point (RH = 74.5% and WSR = 5.2), most of the contact ion pairs transformed into the complex ion aggregates quickly.

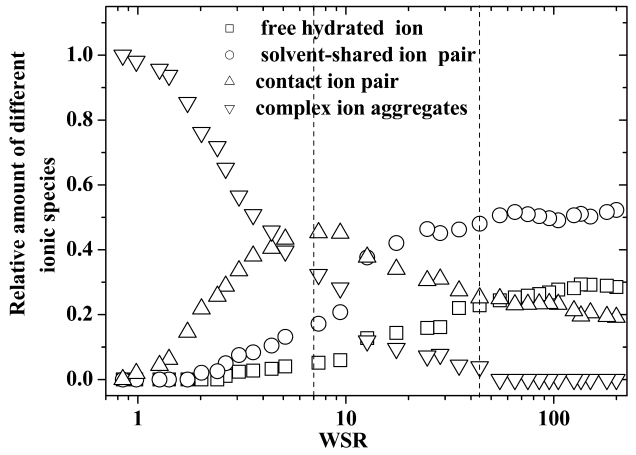

Figure 6. Relative amount of four different ion species in $NaNO_3$ solutions at various WSRs.

Special Ion Structures in Dilute $NaNO_3$ Solution. Electrolyte dissolution in a solution has been studied for decades. Although partial dissociation of electrolyte in the solution was first suggested by Arrhenius long ago,[7] for extended period of time it was believed that in a dilute solution electrolytes would dissociate completely.[9,10,77−79] Debye−Hückel[9] and Onsager[79] thought ions in a dilute solution were perturbed by long-range Coulombic interaction. Meanwhile, Bjerrum[10] proposed the concept of ion pairing of strong electrolytes but claimed the interactions between cation and anion would not exist in a solution made of AB type electrolytes such as NaCl(aq). With the advent of new experimental methods and techniques, more research indicated that strong electrolytes dissociated partially in solutions even at very low concentration.[80−87] In the present study, ion pairs were observed even in highly dilute $NaNO_3$ solutions.

According to Chapados's[80−83] and Dougherty's[84−86] studies of alkali metal halide solutions, two water types exists in electrolyte aqueous solutions, i.e., pure water and salt solvated water. In a electrolytic solution, there are often a fixed amount of solvated water molecules bonded to the salt ions as a cluster, in which cation and anion are solvated and closely bound. As for $NaNO_3$ solution, inner hydrated spheres of Na^+ and NO_3^- have no more than six water molecules.[40,41] On the basis of our Raman spectra, we have found that the interactions between NO_3^- and Na^+ and the resulting formation of ion pairs in the $NaNO_3$ aqueous solution can take place over an extremely wide range of concentration with WSRs from 200 to 0.8. Zhang[24] conducted *ab initio* calculations regarding ion association in $NaNO_3$ solutions and concluded that there are only free hydrated ions and solvent-separated ion pairs (2SIPs) existing in the dilute $NaNO_3$ solution with WSR > 18. However, based on our band component analysis, the spectral information on solvent-shared ion pairs (SIP), contact ion pairs (CIP), and free hydrated ions were derived from the Raman spectra of $NaNO_3$ solutions with WSR between 18 and 200, which are shown in the Figures 5 and 6. The amounts of free hydrated NO_3^- ions, SIPs, and CIPs in dilute solutions with WSR < 35 are 30%, 50%, and 20%, respectively. Within this range, fewer free hydrated ions transformed into SIPs and fewer SIPs transformed into CIPs with a decrease in WSR; as a result, the overall amount of SIPs in solutions was nearly unchanged.

Coupling Vibrations of Water in the Inner Hydration Sphere of Nitrate Ions. During band-component analysis, a band at the frequency of ~1040.0 cm^{-1} was needed to fit the nitrate envelop, as illustrated in the Figure 5. The intensity of the band decreased with the decreasing WSRs over the whole range from 200 to 0.8. According to our *ab initio* calculation results, the band can be attributed to the coupling vibrations of water near NO_3^-. In the calculation, hydrated ions and ion clusters in the aqueous $NaNO_3$ solution were optimized at the HF/6-31+G* level. Based on the optimized models, water molecules in the inner hydration sphere of NO_3^- produced the vibration coupling, and such coupling can only be present in specific structures (Figure 7).

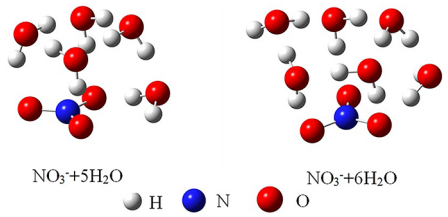

Figure 7. Geometries of optimized hydrated NO_3^- ions and ion pairs.

Temperature-Dependent Raman Spectra of $NaNO_3$ Droplet. Figure 8 shows the Raman shift of ν_1-NO_3^- with ambient temperatures increased from 40 to 80 °C. As seen in the figure, the peak position of ν_1-NO_3^- band had a blue-shift from 1057 to 1061 cm^{-1} accompanied by a slight broadening of fwhm from 15 to 15.5 cm^{-1} as the temperature increased. The changes in the ν_1-NO_3^- band was likely due to the formation of contact ion pairs, especially the complex aggregated contact ions, and this also indicated that cations and anions in the $NaNO_3$/water droplets tend to aggregate with increasing temperatures. Our finding is consistent with the results from Spohn and Brill.[71]

Figure 9 shows peak positions of ν_1-NO_3^- band in $NaNO_3$/water droplets, which were obtained at different temperatures, and the WSRs in the Figure 9 corresponded to those in droplets at room temperature. In our experiments, the droplets deposited on the hydrophobic substrate can reach supersaturated state by lowering RH below the saturation point (RH

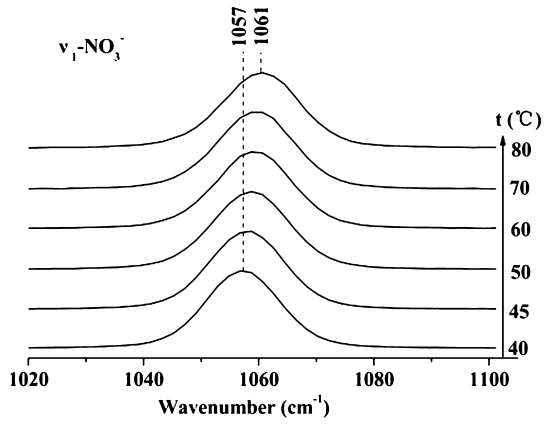

Figure 8. Raman shift of ν_1-NO_3^- in $NaNO_3$/water droplets (~20 mol/L) with temperature in the range 40–80 °C.

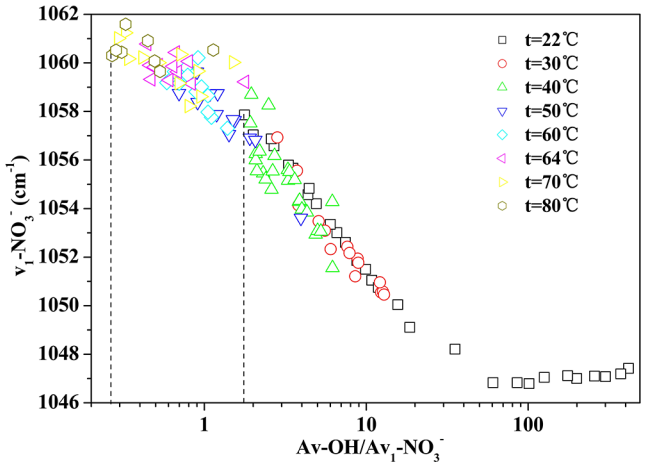

Figure 9. Peak position of the ν_1-NO_3^- band as a function of the area ratio of ν–OH and ν_1-NO_3^- ($A\nu$–OH/$A\nu_1$-NO_3^-) at different temperatures for $NaNO_3$/water droplets.

= 74.5% and WSR = 5.2). At room temperature, the most concentrated solution we obtained was the droplets at RH ~ 27% (WSR ~ 0.8), in which each Na^+ and NO_3^- only shared less than one water molecule. Peak position of the ν_1-NO_3^- band for those droplets is about 1058 cm^{-1} with area ratios of ν–OH and ν_1-NO_3^- ($A\nu$-OH/$A\nu_1$-NO_3^-) approximately equal to 1.77. By increasing the ambient temperature, the area ratios of $A\nu$–OH/$A\nu_1$-NO_3^- of droplets decreased due to loss of water, which was reflected by changes in the concentration of $NaNO_3$ solution, as shown in the Figure 9. The peak position of the ν_1-NO_3^- band shifted to a higher frequency. When ambient temperature increased to ~80 °C, the $A\nu$–OH/$A\nu_1$-NO_3^- decreased to ~0.27 with the ν_1-NO_3^- band shifting to ~1062 cm^{-1}. According to the WSR curve in the Figure 2, the WSR of the most concentrated solution at ~80 °C in this study was estimated to be about ~0.12, and the phase of the $NaNO_3$ droplets was somewhat like anhydrous. With little disturbance from water molecules, cations and anions were highly aggregated and the droplets stayed in the amorphous state, similar to the ionic liquid or melt salt. The melting point of $NaNO_3$ crystal is 306.8 °C under 1 atm pressure, and our study indicated that it may be possible to achieve a state similar to the melt $NaNO_3$ from droplets at 80 °C.

CONCLUSIONS

By using micro-Raman spectroscopy, we have obtained high signal-to-noise ratio spectra of $NaNO_3$ aqueous solutions over a wide concentration range, spanning from highly dilute bulk solutions with WSRs of 200–35 to microdroplets with WSRs of 28–0.8. The droplets deposited on a PTFE substrate can easily reach supersaturated state (WSR < 5.11) by adjusting the ambient RH. With decreasing WSRs from 200 to 0.8, the symmetric stretching band (ν_1-NO_3^-) had a blue-shift of 11 cm^{-1} in the peak position and a broadening of 5.5 cm^{-1} in fwhm, which were attributed to the formation of ion pairs with different structures. The Raman spectra in the range of 1020–1080 cm^{-1} were fitted with Gaussian functions, and five component bands were successfully extracted to derive information on the interactions between Na^+ and NO_3^- ions. Among them, four component bands centered at 1042.9, 1048.5, 1053.5, and 1057 cm^{-1} were respectively assigned to the free hydrated nitrate ions, the solvent-shared ion pairs (SIPs), the contact ion pairs (CIPs), and the complex ion aggregates (CIAs). The last band located at a lower frequency was assigned to the coupling vibration of inner shell hydration water around nitrate ions.

According to our fitting results, amounts of the first four ionic species in $NaNO_3$ solutions changed with increasing concentrations. Besides free hydrated ions, SIPs and CIPs existed in dilute solution even at WSR ~ 200, accounting for ~50% and ~20% of total nitrate species in the WSR range from 45 to 200, respectively. This implied that even in dilute solutions cations and anions tended to congregate together and underwent solvation collectively as they would do in higher concentrations. With WSRs decreasing from 200 to 45, the amount of SIPs kept nearly unchanged along with free decreasing hydrated nitrate ions and increasing CIPs. This was arisen from the transformation of free hydrated nitrate ions to SIPs and further to CIPs at the expense of water molecules. As WSRs decreased further, the amounts of free hydrated nitrate ions and SIPs decreased continuously and reduced to zero at WSR ~ 2. It was also found that CIPs predominated in $NaNO_3$ solutions with WSRs decreased to the range of 9–5, and when WSRs were less than 5, ions aggregated rapidly and formed complex clusters, which eventually led to crystal nucleation.

In addition, the effects of temperature on $NaNO_3$ droplets were studied by Raman spectroscopy at a molecular level. It was found that Na^+ and NO_3^- in droplets tended to aggregate together with each other with increasing temperatures. It was noted that by increasing temperature of $NaNO_3$ droplets, a more concentrated supersaturated state (WSR ~ 0.12) can be achieved and the phase was almost anhydrous. The highly complicated aggregation of cations and anions with little disturbance from water molecules resulted in an amorphous state, which was very similar to that of ionic liquid and melt salt.

ASSOCIATED CONTENT

Supporting Information

Information about the optimized geometries of the complex isomers. This material is available free of charge via the Internet at http://pubs.acs.org.

dx.doi.org/10.1021/jp306367v | J. Phys. Chem. B 2012, 116, 12581–12589

AUTHOR INFORMATION

Corresponding Author

*Tel 86-10-68913596; Fax 86-10-68912652; e-mail yhz@bit.edu.cn (Y.-H.Z.), yong.liu@ucdenver.edu (Y.L.).

Notes

The authors declare no competing financial interest.

ACKNOWLEDGMENTS

Preparation of this manuscript was partially conducted at the Laboratory Directed Research and Development Program at Pacific Northwest National Laboratory (PNNL), a multiprogram national laboratory operated by Battelle for the U.S. Department of Energy (DOE) under Contract DE-AC05-76RL01830, and using EMSL, a national scientific user facility sponsored by the DOE's Office of Biological and Environmental Research (BER) and located at PNNL, while Yunhong Zhang was Alternative Sponsored fellow (ASF).

This work is supported by the NSFC (41175119, 20933001, and 20873006) and 111 project B07012. Yong Liu acknowledges the financial support from Research Corporation for Science Achievement.

REFERENCES

(1) Balabai, N.; Waldeck, D. H. *J. Phys. Chem. B* **1997**, *101*, 2339−2347.
(2) Minofar, B.; Vácha, R.; Wahab, A.; Mahiuddin, S.; Kunz, W.; Jungwirth, P. *J. Phys. Chem. B* **2006**, *110*, 15939−15944.
(3) Fleissner, G.; Hallbrucker, A.; Mayer, E. *J. Phys. Chem.* **1993**, *97*, 4806−4814.
(4) Watanabe, D.; Hamaguchi, H. *J. Chem. Phys.* **2005**, *123*, 034508.
(5) Collins, K. D. *Biophys. J.* **1997**, *72*, 65−76.
(6) Marcus, Y.; Hefter, G. *Chem. Rev.* **2006**, *106*, 4585−4621.
(7) Arrhenius, S. *Z. Phys. Chem.* **1887**, *1*, 631−648.
(8) Szwarc, M. *Acc. Chem. Res.* **1969**, *2*, 87−96.
(9) Debye, P.; Hückel, E. *Phys. Z.* **1923**, *24*, 305−325.
(10) Bjerrum, N. *Z. Elektrochem.* **1918**, *24*, 321−328.
(11) Bjerrum, N. *Mat. Fys. Medd. K. Dan. Vidensk. Selsk.* **1926**, *7*, 1−48.
(12) Duer, W. C.; Robinson, R. A.; Bates, R. G. *J. Chem. Soc., Faraday Trans. 1* **1972**, *68*, 716−722.
(13) Pethybridge, A. D.; Spiers, D. J. *J. Chem. Soc., Faraday Trans. 1* **1977**, *73*, 768−775.
(14) Hanna, E. M.; Pethybridge, A. D.; Prue, J. E. *Electrochim. Acta* **1971**, *16*, 677−686.
(15) Robinson, R. A.; Duer, W. C.; Bates, R. G. *Anal. Chem.* **1971**, *43*, 1862−1865.
(16) Barthel, J.; Neueder, R.; Poepke, H.; Wittman, H. *J. Solution Chem.* **1998**, *27*, 1055−1066.
(17) Kaatze, U.; Hushcha, T. O.; Eggers, F. *J. Solution Chem.* **2000**, *29*, 299−368.
(18) Eigen, M.; Tamm, K. *Z. Elektrochem.* **1962**, *66*, 93−107.
(19) Eigen, M.; Tamm, K. *Z. Elektrochem. Angew. Phys. Chem.* **1962**, *66*, 107−121.
(20) Guo, X.; Shou, J. J.; Zhang, Y. H.; Reid, J. P. *Analyst* **2010**, *135*, 492−502.
(21) Larson, J. W. *J. Phys. Chem.* **1970**, *74*, 3392−3396.
(22) Zhang, H.; Zhang, Y. H. *J. Comput. Chem.* **2010**, *31*, 2772−2782.
(23) Zhang, H.; Zhang, Y. H.; Wang, F. *J. Comput. Chem.* **2009**, *30*, 493−503.
(24) Zhang, H.; Feng, B.; Yu, J. K.; Sun, C. C. *Chem. Res. Chin. Univ.* **2010**, *26*, 656−661.
(25) Xu, M.; Larentzos, J. P.; Roshdy, M.; Criscenti, L. J.; Allen, H. C. *Phys. Chem. Chem. Phys.* **2008**, *10*, 4793−4801.
(26) Hester, R. E.; Grossman, M. E. L. *Inorg. Chem.* **1966**, *5*, 1308−1312.
(27) Vollmarp, P. M. *J. Chem. Phys.* **1963**, *39*, 2236−2248.
(28) Volod'ko, L. V.; Huoah, L. *Zh. Prikl. Spektrosk.* **1968**, *9*, 644−649.
(29) Mathieu, J. P.; Lounsbury, M. *Discuss. Faraday Soc.* **1950**, *9*, 196−207.
(30) Zhang, Y. H.; Choi, M. Y.; Chan, C. K. *J. Phys. Chem. A* **2004**, *108*, 1712−1718.
(31) Hester, R. E.; Plane, R. A. *J. Chem. Phys.* **1964**, *40*, 411−414.
(32) Hester, R. E.; Plane, R. A. *J. Chem. Phys.* **1966**, *45*, 4588−4593.
(33) Irish, D. E.; Nelson, D. L.; Brooker, M. H. *J, Chem. Phys.* **1971**, *54*, 654−657.
(34) Irish, D. E.; Davis, A. R. *Can. J. Chem.* **1968**, *46*, 943−951.
(35) Nelson, D. L.; Irish, D. E. *J. Chem. Phys.* **1971**, *54*, 4479−4489.
(36) Dong, J. L.; Li, X. H.; Zhao, L. J.; Xiao, H. S.; Wang, F.; Guo, X.; Zhang, Y. H. *J. Phys. Chem. B* **2007**, *111*, 12170−12176.
(37) Caminiti, R.; Licheri, G.; Paschina, G.; Piccaluga, G.; Pinna, G. *J. Chem. Phys.* **1980**, *72*, 4522−4528.
(38) Riddell, J. D.; Lockwood, D. J.; Irish, D. E. *Can. J. Chem.* **1972**, *50*, 2951−2962.
(39) Frost, R. L.; James, D. W. *J. Chem. Soc., Faraday Trans. 1* **1982**, *78*, 3249−3261.
(40) Waterland, M. R.; Stockwell, D.; Kelley, A. M. *J. Chem. Phys.* **2001**, *114*, 6249−6258.
(41) Shen, M. Z.; Xie, Y. M.; Schaefer, H. F., III *J. Chem. Phys.* **1990**, *93*, 3379−3388.
(42) Mahoney, J. M.; Stucker, K. A.; Jiang, H.; Carmichael, I.; Brinkmann, N. R.; Beatty, A. M.; Noll, B. C.; Smith, B. D. *J. Am. Chem. Soc.* **2005**, *127*, 2922−2928.
(43) Xu, M.; Tang, C. Y.; Jubb, A. M.; Chen, X. K.; Allen, H. C. *J. Phys. Chem. C* **2009**, *113*, 2082−2087.
(44) Boxe, C. S.; Colussi, A. J.; Hoffmann, M. R.; Perez, I. M.; Murphy, J. G.; Cohen, R. C. *J. Phys. Chem. A* **2006**, *110*, 3578−3583.
(45) Orel, A. E.; Seinfeld, J. H. *Environ. Sci. Technol.* **1977**, *11*, 1000−1007.
(46) Wang, X, B.; Yang, X.; Wang, L. S. *J. Chem. Phys.* **2002**, *116*, 561−570.
(47) Waterland, M. R.; Kelley, A. M. *J. Chem. Phys.* **2000**, *113*, 6760−6773.
(48) Caminiti, R.; Licheri, G.; Piccaluga, G.; Pinna, G. *J. Chem. Phys.* **1978**, *68*, 1967−1970.
(49) Song, C. H.; Carmichael, G. R. *J. Atmos. Chem.* **2001**, *40*, 1−22.
(50) Song, C. H.; Carmichael, G. R. *J. Geophys. Res.* **2001**, *106*, 18131−18154.
(51) Gard, E. E.; Kleeman, M. J.; Gross, D. S.; Hughes, L. S.; Allen, J. O.; Morrical, B. D.; Fergenson, D. P.; Dienes, T.; Galli, M. E.; Johnson, R. J.; et al. *Science* **1998**, *279*, 1184−1187.
(52) Langer, S.; Pemberton, R. S.; Finlayson-Pitts, B. J. *J. Phys. Chem. A* **1997**, *101*, 1277−1286.
(53) Saul, T. D.; Tolocka, M. P.; Johnston, M. V. *J. Phys. Chem. A* **2006**, *110*, 7614−7620.
(54) Hoffman, R. C.; Laskin, A.; Finlayson-Pitts, B. J. *J. Aerosol Sci.* **2004**, *35*, 869−887.
(55) Li, X. H.; Wang, F.; Lu, P. D.; Dong, J. L.; Wang, L. Y.; Zhang, Y. H. *J. Phys. Chem. B* **2006**, *110*, 24993−24998.
(56) Liu, Y.; Yang, Z. W.; Desyaterik, Y.; Gassman, P. L.; Wang, H.; Laskin, A. *Anal. Chem.* **2008**, *80*, 633−642.
(57) Thomas, J. L.; Roeselová, M.; Dang, L. X.; Tobias, D. J. *J. Phys. Chem. A* **2007**, *111*, 3091−3098.
(58) Martin, S. T. *Chem. Rev.* **2000**, *100*, 3403−3453.
(59) Tang, I. N. *J. Geophys. Res.* **1997**, *102*, 1883−1893.
(60) Tang, I. N.; Munkelwitz, H. R. *J. Geophys. Res.* **1994**, *99*, 18801−18808.
(61) Gysel, M.; Weingartner, E.; Baltensperger, U. *Environ. Sci. Technol.* **2002**, *36*, 63−68.
(62) Hemminger, J. C. *Int. Rev. Phys. Chem* **1999**, *18*, 387−417.
(63) Lee, C. T.; Hsu, W. C. *J. Aerosol Sci.* **2000**, *31*, 189−197.
(64) Tang, I. N.; Fung, K. H. *J. Chem. Phys.* **1997**, *106*, 1653−1660.
(65) Ghorai, S.; Tivanski, A. V. *Anal. Chem.* **2010**, *82*, 9289−9298.
(66) Lu, P. D.; Wang, F.; Zhao, L. J.; Li, W. X.; Li, X. H.; Dong, J. L.; Zhang, Y. H.; Lu, G. Q. *J. Chem. Phys.* **2008**, *129*, 104509.

(67) Hu, D.; Qiao, L.; Chen, J.; Ye, X.; Yang, X.; Cheng, T.; Fang, W. *Aerosol Air Qual. Res.* **2010**, *10*, 255−264.
(68) Gibson, E. R.; Hudson, P. K.; Grassian, V. H. *J. Phys. Chem. A* **2006**, *110*, 11785−11799.
(69) Liu, Y. Z.; Pan, D. J. *J. Appl. Opt.* **2010**, *31*, 267−272.
(70) Niedziela, R. F.; Norman, M. L.; DeForest, C. L.; Miller, R. E. *J. Phys. Chem. A* **1999**, *103*, 8030−8040.
(71) Spohn, P. D.; Brill, T. B. *J. Phys. Chem.* **1989**, *93*, 6224−6231.
(72) Wexler, A. S.; Clegg, S. L. *J. Geophys. Res.* **2002**, *107*, 4207−4221.
(73) Clegg, S. L.; Kleeman, M. J.; Griffin, R. J.; Seinfeld, J. H. *Atmos. Chem. Phys.* **2008**, *8*, 1057−1085.
(74) Clegg, S. L.; Brimblecombe, P.; Wexler, A. S. Extended AIM Aerosol Thermodynamic Model, http://www.aim.env.uea.ac.uk/aim/aim.php.
(75) Hudson, P. K.; Schwarz, J.; Baltrusaitis, J.; Gibson, E. R.; Grassian, V. H. *J. Phys. Chem. A* **2007**, *111*, 544−548.
(76) Miller, A. G.; Macklin, J. A. *Anal. Chem.* **1980**, *52*, 807−812.
(77) Sutherland, W. *Philos. Mag.* **1902**, *3*, 161−177.
(78) Davies, C. W. *Ion Association*; Butterworth: London, 1962.
(79) Onsager, L. *Phys. Z.* **1927**, *28*, 277−298.
(80) Max, J. J.; Chapados, C. *J. Chem. Phys.* **2000**, *113*, 6803−6814.
(81) Max, J. J.; Gessinger, V.; Driessche, C.; Larouche, P.; Chapados, C. *J. Chem. Phys.* **2007**, *126*, 184507.
(82) Max, J. J.; Chapados, C. *Can. J. Chem.* **2000**, *78*, 64−72.
(83) Max, J. J.; Chapados, C. *J. Chem. Phys.* **2001**, *115*, 2664−2675.
(84) Dougherty, R. C.; Howard, L. N. *Biophys. Chem.* **2003**, *105*, 269−278.
(85) Dillon, S. R.; Dougherty, R. C. *J. Phys. Chem. A* **2003**, *107*, 10217−10220.
(86) Dillon, S. R.; Dougherty, R. C. *J. Phys. Chem. A* **2002**, *106*, 7647−7650.
(87) Heyrovská, R. *Electroanalysis* **2006**, *18*, 351−361.